EFFICIENCY ANALYSYS OF INFLATION ENVELOPE DEVICES FOR UPPER-STAGE LEO DEORBITING

Alexandru IONEL[1]

This paper analyzes the possibility of implementing an inflation envelope device for deorbiting a launch vehicle upper-stage at end-of-mission from low Earth orbit. The analysis is made through a numerical simulation in MATLAB, in which orbital perturbations such as geopotential, atmospheric drag, direct and indirect solar radiation pressure, are integrated using the ode45 solver. Different envelope sizes are considered, as well as the Earth and Moon shadow effect and the expansion of the gravitational acceleration into spherical harmonics up to J4. A study on similar deorbiting devices is made to better understand the feasibility of implementing this deorbiting technology.

Keywords: inflation envelope, MATLAB numerical simulation, deorbiting device, mitigation rules, deorbiting balloon, ode45, orbital mechanics, orbital perturbations.

1. Introduction

This paper has the purpose of analyzing the performance of a spherical inflation envelope, or balloon, when used as a LEO deorbiting device for an upper-stage at end-of-mission. The performance analysis is made via a MATLAB code, which integrates the equations of motion, including the perturbing accelerations acting on the spacecraft. These accelerations include geopotential, atmospheric drag and direct and indirect solar radiation pressure. It is verified that the deorbiting time meets the ’25 years’ orbital debris mitigation rule. The introduction of the article includes a description of the orbital debris issue and also similar deorbiting devices. Space debris is defined as any human made object in orbit, which is not used in any way. The origin of debris can be inactive spacecraft, rocket fragments, or satellite and launch vehicle parts. The sizes of debris varies from microscopic pieces, to demised spacecraft tens of meters in length. The probability of orbital debris striking and disabling satellites is considered to be low, but it certainly can happen as it has been illustrated in the recent years by a few high profile events. At the moment, the forefront of space management is the prevention of catastrophic damage from space debris or propagating the mass of debris further. [1].

[1] Eng., INCAS - National Institute for Aerospace Research “Elie Carafoli”, Bucharest, Romania, e-mail: alexandru.ionel@incas.ro

2. Inflation deorbiting devices

Inflation structures used as passive deorbiting devices have been studied in various papers. In this research paper, the models and techniques from [2] – [6] will be discussed as examples. In [2], an inflatable reflective balloon acts to lower the perigee through the use of solar radiation pressure, the J2 effect and aerodynamic drag. This paper's conclusion shows that their inflation devices, spherical and conical, are superior to chemical propulsion, and can deorbit CubeSats from the MEO region, being most efficient at 7,000 km altitude. In [3], a 1.22 diameter Mylar balloon, acting as an inflatable aerodynamic brake for deorbiting a single-unit (1U) CubeSat, is investigated. According to [4], a 0.5 meter diameter drag device composed of 0.004" thick Kapton will deorbit a 1U CubeSat from 1000 km in less than 25 years. Other analyzed examples include AeroCube 2 and AeroCube 3 Deorbit Balloons, made from 8 mm thick Kapton and having a 23 cm pillow shape, and 1 mm thick aluminized Mylar, being 0.6 m in diameter. In [5] and [6], the Gossamer Orbit Lowering Device (GOLD) applications include deorbiting CubeSats, defunct satellites, and spent launch vehicle stages. It can be used in LEO to about 1,500 km altitude, increasing cross-sectional area by inflation-maintained ultra-thin envelope which accelerates natural atmospheric drag decay from centuries to months. For example, from an altitude of 833 km, a CubeSat using GOLD could reenter in about 8-12 months at solar mean conditions and in about 4 months at solar max conditions.

3. Numerical simulation methodology

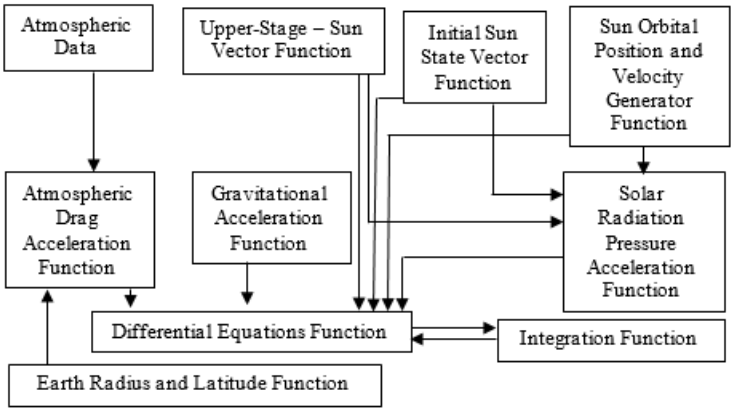

Fig. 1 MATLAB Numerical Simulation Methodology Scheme

The current study focuses on assessing the feasibility of using an inflation envelope (balloon) for deorbiting an upper stage at end-of-mission (EOM) in low Earth orbit (LEO). The numerical investigation is performed via a MATLAB simulation, projecting in time the orbital trajectory of the upper stage equipped with the deorbiting device. The generic scheme of the MATLAB code is shown in Figure 1 and features the functions inside the integration *ode45* function. This MATLAB built in *ode45* solver integrates second order differentials, and is used to integrate with respect to time the accelerations acting upon the spacecraft, namely geopotential, atmospheric drag, solar radiation pressure (SRP) and indirect solar radiation pressure (iSRP). The shadow effect of the Earth and Moon are taken into account.
The equation of motion (1) is integrated by the MATLAB code. The equation uses as initial values the upper-stage state vector (2) and (3).

$$\dot{\boldsymbol{v}}_{us} = \boldsymbol{g_{us}} - \frac{\boldsymbol{v_{us}}}{\|\boldsymbol{v_{us}}\|} a_{drag} + \frac{\boldsymbol{r_{us-Sun}}}{\|\boldsymbol{r_{us-Sun}}\|} a_{SRP} - \frac{\boldsymbol{r_{us}}}{\|\boldsymbol{r_{us}}\|} a_{iSRP} \tag{1}$$

$$\boldsymbol{X}_{us} = \begin{bmatrix} \boldsymbol{r}_{us} \\ \boldsymbol{v}_{us} \end{bmatrix} = \begin{bmatrix} \boldsymbol{x}_{us} \\ \boldsymbol{y}_{us} \\ \boldsymbol{z}_{us} \\ \boldsymbol{v}_{x_{us}} \\ \boldsymbol{v}_{y_{us}} \\ \boldsymbol{v}_{z_{us}} \end{bmatrix} \tag{2}$$

$$\dot{\boldsymbol{X}}_{us} = \begin{bmatrix} \dot{\boldsymbol{r}}_{us} \\ \dot{\boldsymbol{v}}_{us} \end{bmatrix} = \begin{bmatrix} \dot{\boldsymbol{x}}_{us} \\ \dot{\boldsymbol{y}}_{us} \\ \dot{\boldsymbol{z}}_{us} \\ \dot{\boldsymbol{v}}_{x_{us}} \\ \dot{\boldsymbol{v}}_{y_{us}} \\ \dot{\boldsymbol{v}}_{z_{us}} \end{bmatrix} \tag{3}$$

In (1), $\dot{\boldsymbol{v}}_{us}$ represents the total acceleration of the upper-stage on orbit. $\boldsymbol{g_{us}}$ is the gravitational acceleration acting upon the upper-stage. $\boldsymbol{v_{us}}$ is the upper-stage velocity, $\boldsymbol{r_{us-Sun}}$ is the upper-stage – Sun vector, $\boldsymbol{r_{us}}$ is the upper-stage position vector, a_{drag} is the atmospheric drag acceleration, a_{SRP} is the direct solar radiation pressure acceleration magnitude, a_{iSRP} is the indirect solar radiation pressure acceleration magnitude. The constants shown in Table 1 have been used in the calculation of the gravitational acceleration. The constants shown in Table 1 have been used in the calculation of the gravitational acceleration.

Table 1

Constants used in the geopotential model

Mass of Earth	$M_E = 5.972 \cdot 10^{24}\ kg$
Earth Equatorial Radius	$R_E = 6372.137\ km$
Gravitational Constant	$G = 6.673 \cdot 10^{-20}\ \frac{km^3}{kg \cdot s}$
J2 Parameter	$J_2 = 1.08263 \cdot 10^{-3}$
J3 Parameter	$J_3 = -2.5321 \cdot 10^{-6}$
J4 Parameter	$J_4 = -1.610987 \cdot 10^{-6}$

Equations (4) – (15) are components of a function used to calculate the gravitational acceleration having the spacecraft position vector, $\boldsymbol{r_{us}}$, as input, [7], R_{mag} is the magnitude of the upper-stage position vector, $\boldsymbol{z_{us}}$ is the $\boldsymbol{Oz}$ component of the position vector and μ is the gravitational parameter. The function outputs the gravitational acceleration in the x, y, z directions, for which (13), (14) and (15) are used. These outputs are used by the *ode45* solver and integrated with respect to time.

$$R_{mag} = \|\boldsymbol{r_{us}}\| \tag{4}$$

$$R_{R2} = \left(\frac{R_E}{R_{mag}}\right)^2 \tag{5}$$

$$R_{R3} = \left(\frac{R_E}{R_{mag}}\right)^3 \tag{6}$$

$$R_{R4} = \left(\frac{R_E}{R_{mag}}\right)^4 \tag{7}$$

$$z_R = \frac{\boldsymbol{z_{us}}}{R_{mag}} \tag{8}$$

$$z_{R2} = \left(\frac{\boldsymbol{z_{us}}}{R_{mag}}\right)^2 \tag{9}$$

$$z_{R4} = \left(\frac{\boldsymbol{z_{us}}}{R_{mag}}\right)^4 \tag{10}$$

$$q = 1 + 1.5 \cdot J_2 \cdot R_{R2}(1 - 5z_{R2}) + 2.5 \cdot J_3 \cdot R_{R3}(3 - 7z_{R2})z_R - 4.350 \cdot J_4 \cdot R_{R4}\left(9z_{R4} - 6z_{R2} + \frac{3}{7}\right) \tag{11}$$

$$\mu = G_E M_E \tag{12}$$

$$g_x = -\frac{\mu}{R_{mag}^3}\boldsymbol{x_{us}}q \tag{13}$$

$$g_y = -\frac{\mu}{R_{mag}^3}\boldsymbol{y_{us}}q \tag{14}$$

$$g_z = -\frac{\mu}{R_{mag}^2}\left\{\left[\left(1 + 1.5J_2R_{R2}(3 - 5z_{R2})\right)z_R + \left(2.5J_3R_{R3}(6z_{R2} - 7z_{R4} - 0.6)\right) + \left(-4.350J_4R_{R4}\left(\frac{15}{7} - 10z_{R2} + 9z_{R4}\right)z_R\right)\right]\right\} \quad (15)$$

(16) is used for the determination of the acceleration caused by the atmospheric drag force, in which CD is the drag coefficient and ρ is the atmospheric density, with values taken from [8] and [9].

$$a_{Drag} = -\frac{1}{2m}CDA\rho {v_{us}}^2 \frac{\boldsymbol{v_{us}}}{v_{us}} \quad (16)$$

Equation (17), from [10], was used for the calculation of the magnitude of the solar radiation pressure. $\beta = 0.15$ is the coefficient of reflection of reflection of black Kapton, the solar sail material, S_F is the solar flux which was calculated using (18), $P_S = 3.805 \cdot 10^{20}\ W$ is the radiative power of the Sun, r_S is the upper-stage – Sun distance, $a_e = 149.6 \cdot 10^6\ km$ is Earth's semi-major axis in heliocentric orbit, $c = 299\,792.458\ km/s$, A is the surface area of the solar sail, m is the mass of the upper-stage, the solar sail and additional equipment, $a_S = 149 \times 10^6\ km$ is the Sun-Earth semi-major axis.

$$R = (1 + \beta)\frac{S_F}{c}\frac{A\cos\alpha}{m}\left(\frac{a_S}{r_S}\right)^2 \quad (17)$$

$$S_F = \frac{P_S}{4\pi a_e^2} \quad (18)$$

SRP acceleration acting upon the solar sail was considered null when the angle between the Sun-Earth vector and the spacecraft-Earth vector was outside the (-90°, 90°) interval. This was considered because the spacecraft would be pushed outside the orbit, not towards Earth, as necessary. Because the inflated envelope that makes use of SRP to lower the orbit of the upper stage, is spherical, it is considered that at each moment, there is half of sphere facing the Sun. The SRP computed from the semi-sphere surface facing the Sun, is considered to be equal to the sphere cross-sectional area normal to the Sun-Sphere direction. This was also considered for iSRP, with the disc always facing the Earth. For the indirect solar radiation pressure formulation (19) was used, in which $\alpha = 0.367$ is Earth's Albedo, $E_{sun} = 1367\ W/m^2$ is the solar constant, ψ is the angle between the upper-stage and Sun position vectors relative to Earth, [11].

$$R_i(\psi) = \frac{A}{m}\frac{\beta}{c}\frac{\pi R_E E_{sun}}{r_{us}}\left[\frac{2\alpha}{3\pi^2}\left((\pi - \psi)\operatorname{Cos}\psi + \operatorname{Sin}\psi\right) + \frac{1-\alpha}{4\pi}\right] \quad (19)$$

The Sun's state vector is calculated at each instant using (20) and (21) having supplied the initial values $\boldsymbol{r}_{M_0}$ and $\boldsymbol{v}_{M_0}$, [12]. This vector is used throughout the MATLAB code, in the solar pressure functions and shadow effect. f and g in (22) and (23) represent the Lagrange coefficient with $\dot{f}$ and $\dot{g}$ being their time derivatives. $C(z)$ and $S(z)$ are *Stumpff* functions, χ represents the

universal anomaly, which at $t_0 = 0$ is $\chi_{t_0} = 0$. μ_M is the Sun's gravitational parameter and takes the value $\mu_M = G(M_E + M_M)$ with $M_M = 0.0732 \times 10^{24}\ kg$.

$$\boldsymbol{r}_M = f\boldsymbol{r}_{M_0} + g\boldsymbol{v}_{M_0} \tag{20}$$

$$\boldsymbol{v}_M = \dot{f}\boldsymbol{r}_{M_0} + \dot{g}\boldsymbol{v}_{M_0} \tag{21}$$

$$f = 1 - \frac{\chi^2}{r_{M_0}} C(z) \tag{22}$$

$$g = \Delta t - \frac{1}{\sqrt{\mu}} \chi^3 S(z) \tag{23}$$

$$\dot{f} = \frac{\sqrt{\mu}}{r_M r_{M_0}} [z\chi S(z) - \chi] \tag{24}$$

$$\dot{g} = 1 - \frac{\chi^2}{r} C(z) \tag{25}$$

$$z = \frac{1}{a_M} \chi^2 \tag{26}$$

$$S(z) = \begin{cases} \sqrt{z} - \mathrm{Sin}\sqrt{z}, z > 0 \\ \mathrm{Sin}\sqrt{-z} - \sqrt{-z}, z < 0 \\ \frac{1}{6}, z = 0 \end{cases} \tag{27}$$

$$C(z) = \begin{cases} \frac{1-\mathrm{Cos}\sqrt{z}}{z}, z > 0 \\ \frac{\mathrm{Cosh}\sqrt{-z}-1}{-z}, z < 0 \\ \frac{1}{2}, z = 0 \end{cases} \tag{28}$$

$$\chi_{i+1} = \chi_i - \frac{\frac{r_0 v_{r0}}{\sqrt{\mu}} \chi_i{}^2 C(z_i) + \left(1 - \frac{1}{a_M} r_0\right) \chi_i{}^3 S(z_i) + r_0 \chi_i - \sqrt{\mu}\Delta t}{\frac{r_0 v_{r0}}{\sqrt{\mu}} \chi_i \left[1 - \frac{1}{a_M} S(z_i)\right] + \left(1 - \frac{1}{a_M} r_0\right) \chi_i{}^2 C(z_i) + r_0} \tag{29}$$

For the determination of the Sun's initial state vector, the constants in Table 2 were used. For simplicity, it was considered that the Sun orbited the Earth and the Sun was considered to have initially the state vector with opposite sign of the Earth at perigee on the solar orbit.

Table 2

Constants used inside the MATLAB function for calculating the Sun orbital position around the Earth

Mass of Sun	$M_S = 1.989 \cdot 10^{30}\ kg$
Mass of Earth	$M_E = 5.9726 \cdot 10^{24}\ kg$
Global Gravitational Constant	$G = 6.673 \cdot 10^{-20}\ \frac{km^3}{kg \cdot s}$
Earth orbital semi-major axis	$a_S = 149.6 \cdot 10^6\ km$
Earth orbit periapsis	$p_E = 147.09 \cdot 10^6\ km$
Earth orbit apoapsis	$a_E = 152.1 \cdot 10^6\ km$
Earth orbit eccentricity	$e_S = 0.0167$

Earth axis tilt (Sun orbital inclination)	$i_S = 23.4°$
Argument of periapsis	$\omega_S = 102.947°$
Argument of ascending node	$\Omega_S = -11.26°$
Unit vector for non-rotated z axis	$k = [0 \quad 0 \quad 1]$

(30) – (39) present the formulation used for the gravitational parameter (29), the orbital angular momentum calculated at periapsis (30), the velocity of the Sun on orbit at periapsis (31), the initial non rotated position vector (32), the rotation matrix for the argument of periapsis rotation (33), the rotation matrix for the inclination rotation (34), the rotation matrix for the argument of ascending node rotation (35), the rotation equation (36), the equation for rotation around the Z axis (37), and the equation for determining the initial velocity (38).

$$\mu_S = G(M_S + M_E) \tag{30}$$

$$h = \sqrt{p_E \mu_S (1 + e_S \cos 0)} \tag{31}$$

$$v_{pE} = \frac{h}{p_E} \tag{32}$$

$$R_E = [-p_E \quad 0 \quad 0] \tag{33}$$

$$R_\omega = \begin{bmatrix} \cos\omega_S & \sin\omega_S & 0 \\ -\sin\omega_S & \cos\omega_S & 0 \\ 0 & 0 & 1 \end{bmatrix} \tag{34}$$

$$R_i = \begin{bmatrix} 1 & 0 & 0 \\ 0 & \cos i & \sin i \\ 0 & -\sin i & \cos i \end{bmatrix} \tag{35}$$

$$R_\Omega = \begin{bmatrix} \cos\Omega_S & \sin\Omega_S & 0 \\ -\sin\Omega_S & \cos\Omega_S & 0 \\ 0 & 0 & 1 \end{bmatrix} \tag{36}$$

$$R_{RE} = R_\omega R_i R_\Omega R_E \tag{37}$$

$$k_E = R_\omega R_i R_\Omega k \tag{38}$$

$$V_E = v_{pE}\left(\boldsymbol{k_E} \otimes \frac{\boldsymbol{R_E}}{\|\boldsymbol{R_E}\|}\right) \tag{39}$$

The Earth and Moon cylindrical shadow effect acting on the upper-stage was also taken into account, the SRP being considered to be zero, [10]. It was considered that when the angle between the upper-stage – Earth vector and the Sun – Earth vector was between 180-ϕ and 180+ϕ (ϕ is $\sin^{-1}\frac{R_E}{r_{us}}$, where R_E is the Earth radius and r_{us} is the Earth – upper-stage vector magnitude), the upper-stage was in eclipse. Also, the Moon's position in time was calculated using the Lagrange functions. The following algorithm defines the orbital elements, [12], where r is the Earth – Moon distance, v is the Moon's orbital speed, v_r is the Moon's radial speed, $\boldsymbol{h}$ is the Moon's orbital angular

momentum, $\boldsymbol{N}$ is the vector node line of the Moon's orbit, Ω is the right ascension of the ascending node, $\boldsymbol{e}$ is the Moon's orbit eccentricity vector, ω is the Moon's orbit argument of periapsis, θ is the Moon's orbit true anomaly, a is the Moon's orbit semi-major axis, T is the Moon's orbital period and M is the Moon's orbit mean motion.

$$r = \sqrt{\boldsymbol{r} \cdot \boldsymbol{r}} \tag{40}$$

$$v = \sqrt{\boldsymbol{v} \cdot \boldsymbol{v}} \tag{41}$$

$$v_r = \frac{\boldsymbol{r} \cdot \boldsymbol{v}}{r} \tag{42}$$

$$\boldsymbol{h} = \boldsymbol{r} \times \boldsymbol{v} = \begin{vmatrix} \hat{\boldsymbol{\imath}} & \hat{\boldsymbol{\jmath}} & \hat{\boldsymbol{k}} \\ X & Y & Z \\ v_X & v_Y & v_Z \end{vmatrix} \tag{43}$$

$$h = \sqrt{\boldsymbol{h} \cdot \boldsymbol{h}} \tag{44}$$

$$i = \mathrm{Cos}^{-1}\left(\frac{h_Z}{h}\right) \tag{45}$$

$$\boldsymbol{N} = \hat{\boldsymbol{k}} \times \boldsymbol{h} = \begin{vmatrix} \hat{\boldsymbol{\imath}} & \hat{\boldsymbol{\jmath}} & \hat{\boldsymbol{k}} \\ 0 & 0 & 0 \\ h_X & h_Y & h_Z \end{vmatrix} \tag{46}$$

$$N = \sqrt{\boldsymbol{N} \cdot \boldsymbol{N}} \tag{47}$$

$$\Omega = \begin{cases} \mathrm{Cos}^{-1}\left(\frac{N_X}{N}\right), & N_Y \geq 0 \\ 360° - \mathrm{Cos}^{-1}\left(\frac{N_X}{N}\right), & N_Y < 0 \end{cases} \tag{48}$$

$$\boldsymbol{e} = \frac{1}{\mu}\left[\left(v^2 - \frac{\mu}{r}\right)\boldsymbol{r} - r v_r \boldsymbol{v}\right] \tag{49}$$

$$e = \sqrt{\boldsymbol{e} \cdot \boldsymbol{e}} \tag{50}$$

$$\omega = \begin{cases} \mathrm{Cos}^{-1}\left(\frac{\boldsymbol{N} \cdot \boldsymbol{e}}{Ne}\right), & e_Z \geq 0 \\ 360° - \mathrm{Cos}^{-1}\left(\frac{\boldsymbol{N} \cdot \boldsymbol{e}}{Ne}\right), & e_Z < 0 \end{cases} \tag{51}$$

$$\theta = \begin{cases} \mathrm{Cos}^{-1}\left(\frac{\boldsymbol{e} \cdot \boldsymbol{r}}{er}\right), & v_r \geq 0 \\ 360° - \mathrm{Cos}^{-1}\left(\frac{\boldsymbol{e} \cdot \boldsymbol{r}}{er}\right), & v_r < 0 \end{cases} \tag{52}$$

$$a = \frac{h^2}{\mu}\frac{1}{1 - e^2} \tag{53}$$

$$T = \frac{2\pi}{\sqrt{\mu}} a^{\frac{3}{2}} \tag{54}$$

$$M = \frac{2\pi}{T} \tag{55}$$

4. Results and discussion

In Table 4, the numerical simulation results are presented, showing the deorbiting time necessary to deorbit a 418 kg upper-stage from 600 km and 1400 km, using 25 m, 50 m and 100 m radii deorbiting balloons. As it can be seen from these results, the larger radii balloons are most efficient from either 600 or 1400 km, but even the smaller radius balloons deorbit the upper-stage respecting the ’25 years’ mitigation rule.

Table 3

Numerical simulation results - deorbiting time for 25m, 50m and 100m radius deorbiting balloons used from starting altitudes of 600 km and 1400 km

Deorbiting altitude [km]	Balloon radius [m]	Deorbiting time
600	25	18 days
600	50	5 days
600	100	2 days
1400	25	46 days
1400	50	13 days
1400	100	4 days

In Fig. 2 the deorbiting time for balloons with 25m, 50m and 100m is presented, when deorbiting from a starting altitude of 600 km. In Fig. 3 the SRP acceleration variation for balloons with 25m, 50m and 100m radii is presented, when deorbiting from a starting altitude of 600 km.

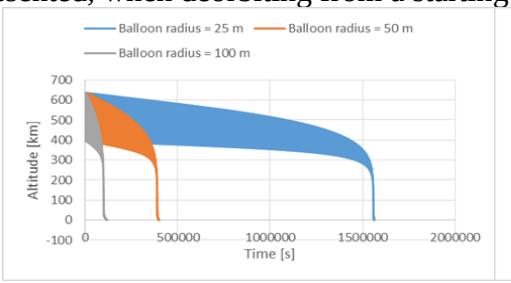

Fig. 1 Deorbiting time for balloons with different radii, when used from a 600 km initial altitude

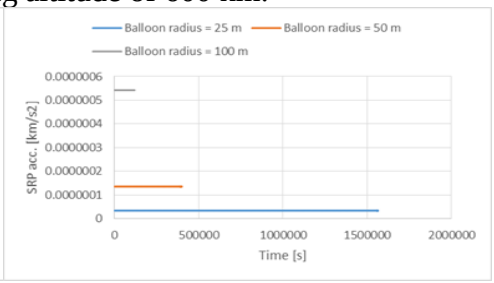

Fig. 2 SRP values for deorbiting balloon with different radii, when used from a 600 km initial altitude

In Fig. 4 the iSRP acceleration variation for balloons with 25m, 50m and 100m radii is presented, when deorbiting from a starting altitude of 600 km. In Fig. 5 the atmospheric drag acceleration variation for balloons with 25m, 50m and 100m radii is presented, when deorbiting from a starting altitude of 600 km.

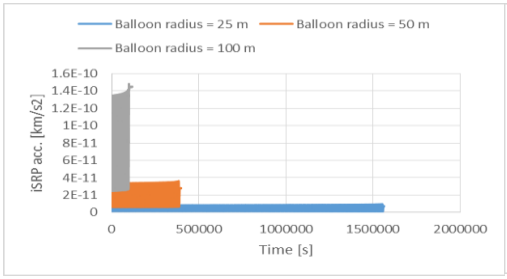

Fig. 3 Indirect SRP Acceleration values for deorbiting balloons with different radii, when used from a 600 km initial altitude

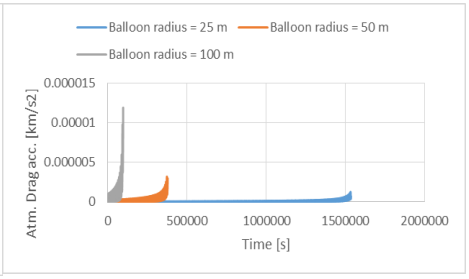

Fig. 4 Atmospheric Drag Acceleration values for deorbiting balloons with different radii, when used from a 600 km initial altitude

In Fig. 6 the altitude acceleration variation for balloons with 25m, 50m and 100m radii is presented, when deorbiting from a starting altitude of 1400 km. In Fig. 7 the SRP acceleration variation for balloons with 25m, 50m and 100m radii is presented, when deorbiting from a starting altitude of 1400 km.

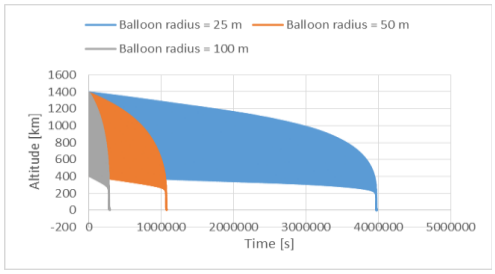

Fig. 5 Deorbiting time for balloons with different radii, when used from a 1400 km initial altitude

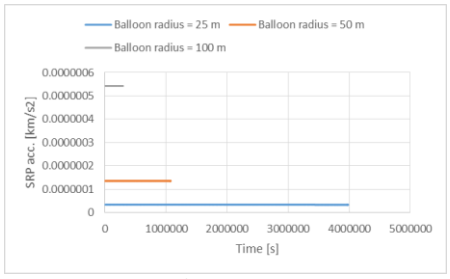

Fig. 6 SRP values for deorbiting balloons with different radii, when used from a 1400 km initial altitude

In Fig. 8 the iSRP acceleration variation for balloons with 25m, 50m and 100m radii is presented, when deorbiting from a starting altitude of 1400 km. In Fig. 8 the atmospheric drag acceleration variation for balloons with 25m, 50m and 100m radii is presented, when deorbiting from a starting altitude of 1400 km.

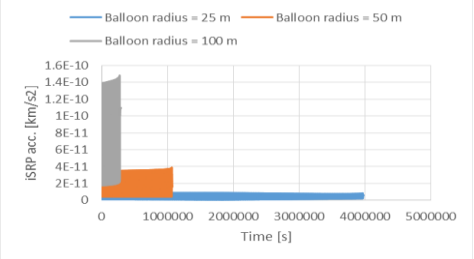

Fig. 7 Indirect SRP Acceleration values for deorbiting balloons with different radii, when used from a 1400 km initial altitude

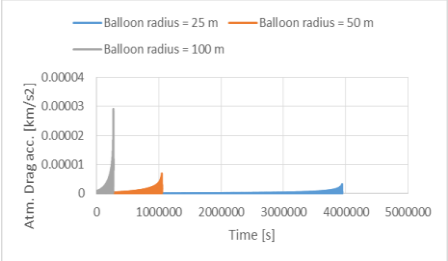

Figu. 8 Atmospheric Drag Acceleration values for deorbiting balloons with different radii, when used from a 1400 km initial altitude

For a detailed analysis of the perturbing action of SRP, iSRP and atmospheric drag onto the spacecraft equipped with the balloon deorbiting device, the main orbital elements variation over the course of the deorbiting is given in Figs. 10-14, for the balloon with a 25 m radius, when deorbiting from 1400 km altitude. In Fig. 10 the inclination variation for balloon with 25m radius is presented, when deorbiting from a starting altitude of 1400 km. In Fig. 11 the argument of periapsis variation for balloons with 25m, 50m and 100m radii is presented, when deorbiting from a starting altitude of 1400 km. In Fig. 12 the RAAN variation for a deorbiting balloon with 25m radius is presented, when deorbiting from a starting altitude of 1400 km. In Fig. 13 the true anomaly acceleration variation for a deorbiting balloon with a 25m radius is presented, when deorbiting from a starting altitude of 1400 km.

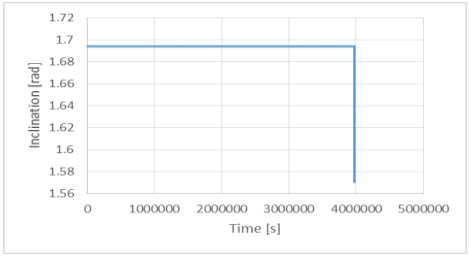

Fig. 9 Inclination variation in the case of using a 25 m radius balloon from an initial altitude of 1400 km

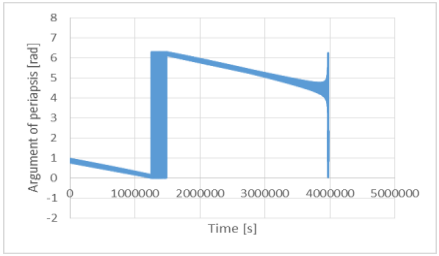

Fig. 10 Argument of periapsis variation in the case of using a 25 m radius balloon from an initial altitude of 1400 km

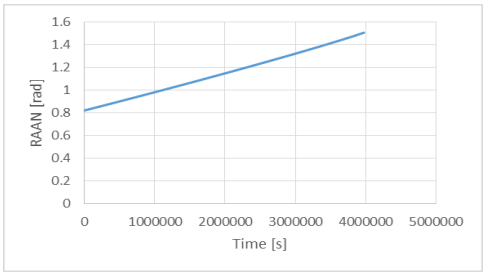

Fig. 11 RAAN variation in the case of using a 25 m radius balloon from an initial altitude of 1400 km

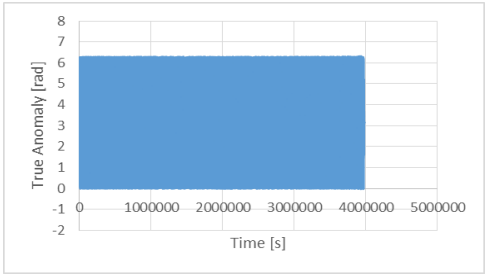

Fig. 12 True anomaly variation in the case of using a 25 m radius balloon from an initial altitude of 1400 km

5. Conclusions

This paper has concluded that deorbiting inflation envelopes (balloons) are efficient in deorbiting a 418 upper-stage from 600 km and 1400 km, and meeting the ’25 years’ mitigation rule. The best results were obtained for the 100 m radius balloon, which deorbited the upper-stage from 1400 km altitude in 4 days.

REFERENCES

[1] *T. Muelhaupt*, Space Debris and The Aerospace Corporation, Crosslink, Vol. 16, No. 1, 2015.
[2] *C. Lucking*, A Passive High Altitude Deorbiting Strategy.
[3] *A. Kim, C. Branco, D. Warner, E. Billips, L. Lewis, M. Webb, B. Crawse, J. Harris, A*. Streit, Design and Development of a CubeSat De-Orbit Device, Final Report MAE 435.
[4] *M. Roddy*, Development of a Solid-State Inflation Balloon for Aerodynamic Drag Assisted Deorbit of CubeSats.
[5] *J. K. Fuller, D. Hinkley, S. W. Janson*, CubeSat Balloon Drag Devices: Meeting the 25-Year De-Orbit Requirement, Physical Science Laboratories, August, 2010.
[6] *N. S. Amade, K. T. Nock, K. Aaron, B. Goldman*, Gossamer Orbit Lowering Device (GOLD) for Safe and Efficient CubeSat Deorbit, CubeSat Workshop, Logan, UT, August 8-9, 2015.
[7] *A. Tewari*, Atmospheric and Space Flight dynamics
[8] *W. S. K. Champion, E. A. Cole and J. A. Kantor*, Standard and Reference Atmospheres, Handbook of Geophysics and the Space Environment, Chapter 14, 2003.
[9] * * * NASA, U.S. Standard Atmosphere, 1976, N77-16482
[10] *D. G. Cook*, Solar Radiation Pressure Modelling Issues for High Altitude Satellites
[11] *S. Lupu, E. Zaharescu*, Effects of Direct and Indirect Solar Radiation Pressure in Orbital Orbital Parameters of GPS Satellites
[12] *H. Curtis*, Orbital Mechanics for Engineering Students.